Surg Radiol Anat (2016) 38:557–561
DOI 10.1007/s00276-015-1561-1

Proposed three-dimensional model of the orbit and relevance to orbital fracture repair

Alexander Fitzhugh[1] · Hasan Naveed[1] · Indran Davagnanam[2] · Ashraf Messiha[3]

Received: 21 February 2015 / Accepted: 26 September 2015 / Published online: 25 November 2015

Abstract
Purpose To describe the relationship of the orbital rim and depth in Far Eastern skulls by anatomical study, using morphometry to yield an octagonal three-dimensional model of the orbit.
Methods Forty-one orbits of 21 Far Eastern skulls from the Department of Anatomy of St George's, University of London were included in this study. A morphometric study was conducted, measuring between eight reproducible orbital rim landmarks to yield perimeters, and from these landmarks to the optic canal to yield orbital depth. Orbital height and width were also recorded. Results were statistically analysed to look for evidence of gender variation or laterality before comparison with those from other ethnicities. The authors then present a method for three-dimensional description of the orbit.
Results 67 % of orbits were male. Orbital height and width were significantly greater in males (34.6 ± 2.0 and 39.4 ± 1.7, vs. 32.5 ± 2.3 and 37.2 ± 2.4 mm). Orbital perimeter tended towards being larger in males (126.3 vs. 122.2 mm, $p = 0.05$), as was the angle between medial and lateral walls (50.1° ± 2.0°, vs. 47.9° ± 3.0°).
Conclusion This study has proposed a new method for describing the orbit using three-dimensional measurements, yielding clinically useful morphometric data. These results and model have applications in surgical navigation of the orbit, repair of fractures, and prediction of post-traumatic or surgical enophthalmos.

Keywords Orbit · Fractures · Repair · Model · Radiological · Enophthalmos

Introduction

Orbital fractures are a common complication following facial trauma [3]. There are generally two components to each injury; disruption to the orbital rim, with half involving the zygomatic complex, and disruption to one or more orbital walls [10]. Extensive fractures involving the mid-face and the orbit may lead to an increase in orbital volume with subsequent enophthalmos [4], with repair indicated for correction of diplopia, enophthalmos, and for clinical or radiological evidence of entrapment [3].

The proximity of the neurovascular structures in the congested orbital space requires a detailed working knowledge of the morphometric and geometric relationships between the osteological landmarks at the rim, and towards the orbital apex. Literature has established that orbital anatomy varies between genders and ethnicities by comparing morphometry and orbital volume [6–8, 12]. However, few studies have attempted to relate rim morphometry to orbital wall depth, which has clinical use in operative planning, enophthalmos correction, and classification of injuries.

Our study aimed to demonstrate use of rim and depth measurements to yield a simple three-dimensional model of the orbit as an octagonal pyramid. Data were then compared with other studies to validate our model, and a radiological technique for describing the orbit and its uses is then

✉ Ashraf Messiha
messihaashraf@icloud.com

[1] Division of Biomedical Sciences (Anatomy), St George's, University of London, London, UK

[2] Brain Repair and Rehabilitation Unit, UCL Institute of Neurology, London, UK

[3] Maxillofacial Unit, St George's Hospital NHS Trust, London, UK

presented. Our results are likely to be of interest to surgeons in cases of orbital fracture repair, and to radiologists in accurately classifying the location of orbital defects.

Materials and method

41 orbits, from a total of 21 dry skulls were included in the study. All specimens were selected from skeletal collections belonging to the Department of Anatomy of St George's, University of London. Specimens were determined for gender and ethnicity by a forensic anthropologist using macroscopic cranial–facial features based on anthropological research, though age was unknown. Criteria used and references are described in the Museum of London's 'Human Osteology Method Statement' [1].

Reproducible orbital rim landmarks were identified for measurement (Fig. 1). These included: supraorbital notch/foramen; zygomatico-frontal suture; zygomatico-maxillary suture; most inferior point of the inferior–anterior lacrimal crest. These were chosen as they were both visually determinable, and based on previous morphometric literature to ensure comparison of results. The authors appreciate that suture and foramina position may vary between paired orbits. However, existing studies do not demonstrate significant laterality between paired orbits as a result [6–8, 12].

Other landmarks were chosen based on ease of identification and were: midway between supraorbital notch/foramen and zygomatico-frontal suture; most inferior point of the lateral orbital rim, intersection point of Frontomaxillary suture and orbital rim; most Superior point of medial orbital rim.

Distance measurements between the anatomical landmarks were recorded three times using a surgical ruler and averaged. Measurements were taken between the eight orbital rim perimeter distances (P1–P8), and from these eight rim positions to the edge of the orbital foramen, corresponding to orbital depths (D1–D8), allowing the orbit to be conceptualised as an irregular octagonal pyramid (Fig. 1). Orbital wall boundaries were defined as: superior (rim P1 + P2 + P8); lateral (rim P3); inferior (rim P4 + P5); medial (rim P6 + P7). Measurements were also made of orbital height, taken as a vertical measurement from most inferior aspect of the rim upwards, and orbital width, taken from the most medial to most lateral orbital rim. Width measurements were combined with their respective lateral and medial depth measurements (D3 and D7) to form a triangle allowing calculation of the horizontal angle between the two walls. Further calculations were made of each individual triangular segment of the orbital wall using Heron's formula to estimate surface areas for the orbital walls. Microsoft Excel package was used to tabulate data and to conduct *T*-tests for analysis of statistical significance. *p* values of <0.05 were considered significant.

Results

Of the 21 skulls included, 14 (67 %) were anthropologically determined male, and all anthropologically 'Far Eastern'. Data were compared between right and left orbits,

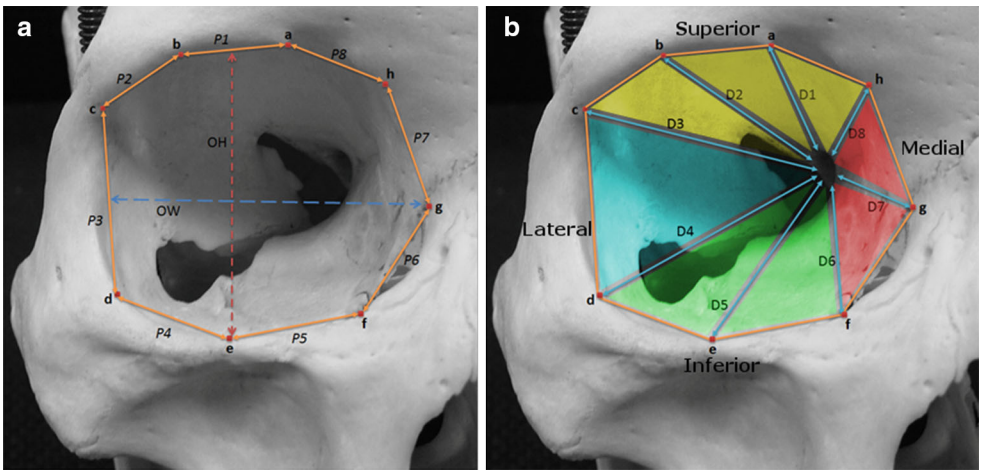

Fig. 1 Methodology for recording orbital rim (**a**) and depth measurements (**b**). Anterior views of right orbit showing 8 landmarks at the orbital rim: *a* supraorbital notch/foramen, *b* midpoint between supraorbital notch/foramen and zygomatico-frontal suture, *c* zygomatico-frontal suture, *d* most inferior point of lateral orbital rim, *e* zygomatico-maxillary suture, *f* most inferior point of the anterior lacrimal crest, *g* intersection point of frontomaxillary suture and orbital rim, *h* most superior point of medial orbital rim. Orbital height (*OH*) is taken as a vertical measurement from most inferior aspect of the rim upwards whilst orbital width (*OW*) represents the most medial to most lateral orbital rim. These landmarks were used to calculate perimeter measurements (P1–P8) at the orbital rim, orbital height and width. The depth measurements (*D1–D8*) were also recorded with respect to the optic foramen's edge. The orbital rims can be defined as per our model: superior (rim *P1* + *P2* + *P8*); lateral (rim *P3*); inferior (rim *P4* + *P5*); medial (rim *P6* + *P7*)

Table 1 Measurements from Far Eastern Skulls

	Male		Female		Comparison
	Length	SD	Length	SD	*p* value
Orbital height (mm)	34.6	±2.0	32.5	±2.3	0.008*
Orbital width (mm)	39.4	±1.7	37.2	±2.4	0.007*
Horizontal angle (°)	50.1	±2.0	47.9	±3.0	0.02*
Perimeter (mm)	126.3	±6.5	122.2	±6.1	0.05
Superior (D1) (mm)	50.1	±1.9	50.8	±2.4	0.3
Lateral (D3) (mm)	47.4	±2.6	47.4	±2.6	1.0
Inferior (D5) (mm)	48.0	±1.9	47.9	±3.0	0.9
Medial (D7) (mm)	45.1	±2.3	44.0	±2.5	0.2
	Right		Left		Comparison
	Length	SD	Length	SD	*p* value
Orbital height (mm)	34	±2.4	33.8	±2.3	0.4
Orbital width (mm)	38.7	±2.2	38.7	±2.3	0.9
Horizontal angle (°)	49.4	±2.2	49.4	±3.0	0.4
Perimeter (mm)	124.2	±6.2	125.6	±7.1	0.2
Superior (D1) (mm)	50.3	±2.1	50.4	±2.2	0.7
Lateral (D3) (mm)	47.1	±2.5	47.7	±2.7	0.02*
Inferior (D5) (mm)	48.1	±2.4	47.9	±2.3	0.6
Medial (D7) (mm)	44.7	±2.4	44.7	±2.5	0.9
	Combined (both sides)				
	Length		SD		
Orbital height (mm)	33.9		±2.3		
Orbital width (mm)	38.7		±2.2		
Horizontal angle (°)	49.4		±2.6		
Perimeter (mm)	124.9		±6.6		
Superior (D1) (mm)	50.3		±2.1		
Lateral (D3) (mm)	47.4		±2.6		
Inferior (D5) (mm)	48.0		±2.3		
Medial (D7) (mm)	44.7		±2.4		

SD standard deviation, *HA* horizontal angle calculated between D3 and D7

* Statistical significance with *T* test

looking for evidence of laterality, and male and female orbits using paired and unpaired student's *T*-tests, respectively. Results are summarised in Tables 1 and 2.

Both height and width (mean in mm ± standard deviation) were significantly greater in men compared to women (34.6 ± 2.0 and 39.4 ± 1.7, vs. 32.5 ± 2.3 and 37.2 ± 2.4 mm), as was horizontal angle (50.1° ± 2.0°, vs. 47.9° ± 3.0°). Orbital wall length demonstrated no gender difference, but lateral wall depth showed significant laterality ($p = 0.02$). Orbital perimeter tended towards being significantly larger in males (126.3 vs. 122.2 mm, $p = 0.05$), although there was no evidence of laterality.

Table 2 Orbit perimeters and calculated wall surface areas

	Male		Female	
	Value	SD	Value	SD
Sup (P1 + 2 + 8) (mm)	42.3	±3.2	41.7	±2.5
Lat (P3) (mm)	22.0	±1.8	21.3	±1.8
Inf (P4 + 5) (mm)	30.4	±3.1	31.0	±2.2
Med (P6 + 7) (mm)	31.4	±3.2	28.2	±3.3
Sup area (mm^2)	1021.6	±100.2	1008.5	±73.1
Lat area (mm^2)	515.6	±41.3	497.3	±45.0
Inf area (mm^2)	712.0	±90.9	718.6	±90.0
Med area (mm^2)	692.3	±78.8	601.4	±84.3
	Right		Left	
	Value	SD	Value	SD
Sup (P1 + 2 + 8) (mm)	39.6	±9.7	43.0	±2.7
Lat (P3) (mm)	21.8	±1.8	22.1	±1.7
Inf (P4 + 5) (mm)	28.9	±7.2	30.9	±3.4
Med (P6 + 7) (mm)	28.6	±7.5	30.5	±4.1
Sup area (mm^2)	1000.4	±90.0	1033	±91.4
Lat area (mm^2)	502.7	±39.7	515.6	±45.8
Inf area (mm^2)	705.8	±78.7	722.3	±100.1
Med area (mm^2)	658.2	±80.5	663.5	±101.1
	Combined (both sides)			
	Value		SD	
Sup (P1 + 2 + 8) (mm)	42.2		±3.0	
Lat (P3) (mm)	21.8		±1.8	
Inf (P4 + 5) (mm)	30.6		±2.8	
Med (P6 + 7) (mm)	30.3		±3.6	
Sup area (mm^2)	1017.1		±91.1	
Lat area (mm^2)	509.3		±42.9	
Inf area (mm^2)	714.2		±89.5	
Med area (mm^2)	661.2		±90.8	

P# individual perimeter length, *D#* individual depth value, *Sup* superior wall, *Lat* lateral wall, *Inf* inferior wall, *Med* medial wall

* Statistical significance with *T*-test

Discussion

The morphometric data obtained were comparable with those of other studies describing Far Eastern orbits; especially Chinese. Values for height and width resembled Ji et al. [7], but were smaller compared to Korean skulls [6]. Results from a European population gathered by CT demonstrated significant gender difference for both values but only after adjusting data for subject height [12]. Orbital perimeter was similar between our data and Ji et al. for males and females, suggesting that our method of using eight orbital rim landmarks is an accurate substitute for more complex arc-based measurements, despite suture and foramina variability.

Orbital depth measurements were comparable between our data and Chinese skulls, but were larger than those of Koreans [6]. Our values were greater than Karakaş et al's European skulls [8], except for the inferior value, which included height from the infraorbital foramen. Since we used the intersection point of frontomaxillary suture and orbital rim rather than the anterior lacrimal crest, this is the likely cause for differences in medial measurements.

Horizontal angle is less often presented in literature, though Borumandi et al. reported a mean angle of $50.2° \pm 4.1°$ [2], comparable to a mean value of $49.4° \pm 2.6°$ with our technique, suggesting this approximation is acceptable.

Traditionally, the orbit has been conceptualised as a quadrilateral pyramid consisting of a broad base and four walls, which converge at the apex. However, the orbit is clearly a more complex three-dimensional structure. We suggest that by combining rim and depth measurements, the orbit can be modelled as an octagonal pyramid.

Three-dimensional models provide large amounts of data, but are not necessarily as digestible as simpler polygonal models. Our eight-sided model enables an accurate method of describing the walls' contours whilst remaining clinically applicable to fractured orbits requiring surgical reconstruction.

Enophthalmos is the most common complication following traumatic orbital volume change injury, affecting around 30 % of patients, of which 7 % will persist despite reconstruction [5]. Additionally, the orbital surgeon often encounters optic neuropathy, persistent diplopia, extraocular muscle entrapment or retrobulbar haemorrhage in severely injured orbits [3–5]. Therefore, timely and accurate repair of both the rim and wall is imperative to ensure stability and restoration of orbital volume fracture.

In such cases of orbital trauma, we suggest the use of our three-dimensional model in assessing and managing orbital reconstruction. The use of reproducible osteological landmarks in our methodology allows our model to be translated to orbital CT scans. We recommend using 0.75 mm slice CT reconstructions standardised to bone algorithm setting, which can be manipulated to generate two-dimensional sections and three-dimensional models.

The clinical application of our model predominantly applies to unilateral orbital injuries. The octagonal pyramidal model generated on the contralateral intact orbit can be mirrored and superimposed on the fractured orbit to generate a symmetric map composed of eight triangular components of the octagonal pyramid. The different subunits help to map the traumatic defect, aiding in accurately classifying the position of displaced bones. Additionally, the relative area of each subunit (calculated using Heron's formula) provides the restorative dimensions, aiding mesh plate and bone graft customisation. This minimises undercutting or overcutting in shaping the appropriately sized scaffold.

The application of the model can also provide a volume measure based on relatively consistent landmarks, useful in the prediction of enophthalmos. Kolk et al. have demonstrated that 0.93 mm of enophthalmos develops for a change of 1 cm^3 at 3–4 months [9]. The authors propose the use of the following method to calculate the geometric volume with CT (Fig. 2). The volume of an irregular octagonal pyramid can be calculated by:

$$(1/3) \times (\text{base area at the orbital rim}) \times (\text{height of the pyramid from base to apex})$$

The orbital rim's base area is contained by the eight rim points, and can either be calculated using 3D reconstructions in standard CT imaging software, or approximated using a polygonal area measurement tool on a slightly angulated coronal plane.

Given the relative angulation of the medial and lateral orbital walls is 50° (Fig. 2a), tilting the sagittal axis at 25° to the midline would provide a central cross-sectional view of the orbital depth (Fig. 2b). This view can be used to

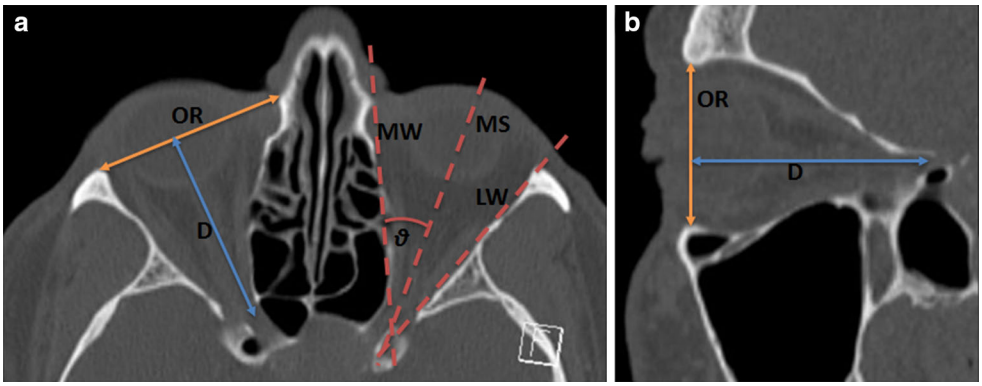

Fig. 2 Methodology for recording orbital depth using CT. A mid-orbital axial view (**a**) allows visualisation of both the medial (*MW*) and lateral (*LW*) orbital walls, lying at an angulation of 50°. This view can be used to calculate the mid-sagittal section at 25° (here seen as θ). This sagittal section (**b**) shows the most posterior edge of the optic canal and anterior edge of the orbital rim (*OR*). The distance between these two yields the depth measurement (*D*)

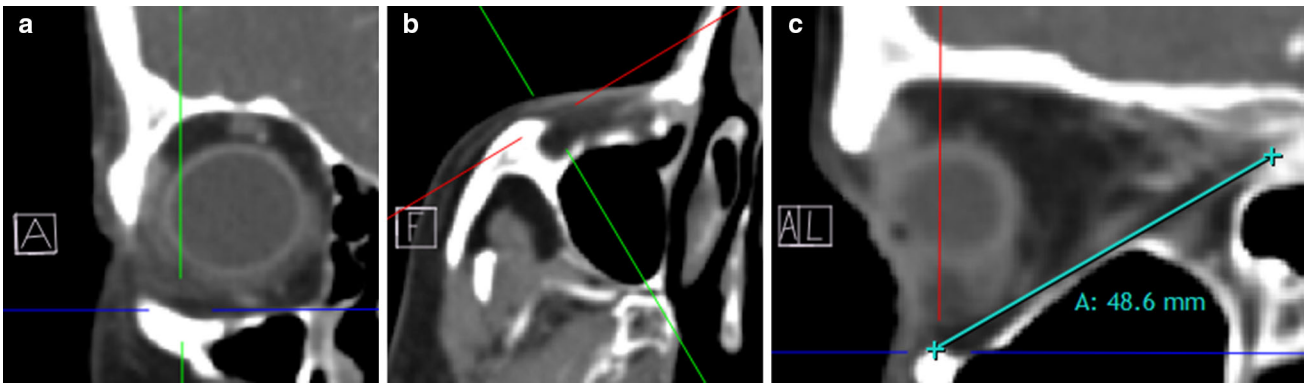

Fig. 3 Application of the octagonal model to CT images. Firstly the orbital rim landmark is identified using a coronal view (**a**), for example point 'd' (most inferior point of lateral orbital rim). Using multiplanar reconstruction, an oblique section is drawn from here to the nearest edge of the optic canal (**b**). A measurement can then be taken along this plane (**c**) to yield depth D3

measure orbital height from the plane of the orbital base (line connecting supraorbital ridge to infraorbital ridge) to the midpoint of the optic foramen. Depth and perimeter values of the model can be calculated using multiplanar reconstruction (Fig. 3).

Applying the model to the contralateral intact orbit can provide a baseline volume, which can be compared with post-surgical and post-traumatic volumetric changes in the fractured orbit [11]. This method has the advantage over more accurate volume-calculating software by virtue of its speed, affordability and simpler clinical application, though it is appreciated that as a consequence of this, such volumes will be inherently less accurate.

Limitations of our study included our inability to adjust for orbit remodelling with age, the male skull predominance, lack of exact ethnic origin, and that bone scale may vary across times (for example due to nutrition). As such, our geometric model may not be applicable to all races and genders.

Acknowledgments The authors would like to thank Jelena Bekvalac, Curator of Human Osteology at the Museum of London, for her time and expertise in forensically evaluating the specimens.

Compliance with ethical standards

Ethical standards The authors confirm that this work has been conducted in accordance with the laws of the United Kingdom, where it was performed.

Conflict of interest The authors declare that they received no funding for this research. Messiha is currently employed by St George's Hospital. Fitzhugh and Naveed have previously received payment for employment by St George's Medical School, for work unrelated to this research.

References

1. Bekvalac J (2012) Sex determination. In: Powers N (ed) Human osteology method statement. Museum of London. Available via Museum of London. http://archive.museumoflondon.org.uk/NR/rdonlyres/3A7B0C25-FD36-4D43-863E-B2FDC5A86FB7/0/OsteologyMethodStatementrevised2012.pdf. Accessed 11 Aug 2015
2. Borumandi F, Hammer B, Noser H, Kamer L (2013) Classification of orbital morphology for decompression surgery in Graves' orbitopathy: two-dimensional versus three-dimensional orbital parameters. Br J Ophthalmol 97(5):659–662. doi:10.1136/bjophthalmol-2012-302825
3. Burnstine MA (2003) Clinical recommendations for repair of orbital facial fractures. Curr Opin Ophthalmol 14(5):236–240
4. Gentile MA, Tellington AJ, Burke WJ, Jaskolka MS (2013) Management of midface maxillofacial trauma. Atlas Oral Maxillofac Surg Clin North Am 21(1):69–95. doi:10.1016/j.cxom.2012.12.010
5. Hoşal BM, Beatty RL (2002) Diplopia and enophthalmos after surgical repair of blowout fracture. Orbit 21(1):27–33. doi:10.1076/orbi.21.1.27.2598
6. Hwang K, Baik SH (1999) Surgical anatomy of the orbit of Korean adults. J Craniofac Surg 10(2):129–134
7. Ji Y, Qian Z, Dong Y, Zhou H, Fan X (2010) Quantitative morphometry of the orbit in Chinese adults based on a three-dimensional reconstruction method. J Anat 217(5):501–506. doi:10.1111/j.1469-7580.2010.01286.x
8. Karakaş P, Bozkir MG, Oguz O (2003) Morphometric measurements from various reference points in the orbit of male Caucasians. Surg Radiol Anat 24(6):358–362. doi:10.1007/s00276-002-0071-0
9. Kolk A, Pautke C, Schott V, Ventrella E, Wiener E, Ploder O, Horch HH, Neff A (2007) Secondary post-traumatic enophthalmos: high-resolution magnetic resonance imaging compared with multislice computed tomography in postoperative orbital volume measurement. J Oral Maxillofac Surg 65(10):1926–1934. doi:10.1016/j.joms.2006.06.269
10. Manolidis S, Weeks BH, Kirby M, Scarlett M, Hollier L (2002) Classification and surgical management of orbital fractures: experience with 111 orbital reconstructions. J Craniofac Surg 13(6):726–737
11. Tahernia A, Erdmann D, Follmar K, Mukundan S, Grimes J, Marcus JR (2009) Clinical implications of orbital volume change in the management of isolated and zygomaticomaxillary complex-associated orbital floor injuries. Plast Reconstr Surg 123(3):968–975. doi:10.1097/PRS.0b013e318199f486
12. Weaver AA, Loftis KL, Tan JC, Duma SM, Stitzel JD (2010) CT based three-dimensional measurement of orbit and eye anthropometry. Invest Ophthalmol Vis Sci 51(10):4892–4897. doi:10.1167/iovs.10-5503